A novel dimensionless index for optimizing the thermo-hydraulic performance of steam condensation in horizontal rotating channels of a multi-channel cylinder dryer

SHA WANG, HAOZENG GUO, AND JIANYONG WANG

ABSTRACT: The comprehensive performance of steam condensation in horizontal rotating channels, which involves a trade-off between heat transfer enhancement and flow resistance, lacks a unified evaluation criterion. This deficiency is particularly critical for applications such as a multi-channel cylinder dryer (MCD) in paper machines, where rotational operation enhances drying efficiency. To address this gap, this study introduces a novel dimensionless index, *W/Eu*, defined as the ratio of the dimensionless heat transfer coefficient (*W*) to the dimensionless pressure drop (*Eu*), thereby taking into account both heat transfer and flow resistance characteristics comprehensively. A functional relationship for this index was established with respect to channel spacing (W_r) and steam mass flux (G), followed by a theoretical optimization analysis.

The analysis reveals that *W/E*u decreases monotonically as W_r increases and increases monotonically as G increases, ultimately diverging as $G \to \infty$. Consequently, for any given operational range, the theoretical maximum performance is achieved at the boundary condition of minimum channel spacing ($W_r \to 0$) and maximum allowable mass flux ($G = G_{max}$). This work provides a clear theoretical directive for the design and optimization of high-efficiency rotating heat exchanger systems, offering valuable insights for enhancing the drying performance of microchannel dryers in paper machines and similar rotary thermal systems.

Application: This work provides theoretical guidance for the design of next-generation MCD, while also paving the way for more efficient and sustainable paper production technologies.

As an energy-intensive industry, the paper manufacturing sector consumes over 50% of its total operational energy in the drying section alone. Thus, improving the efficiency of the drying cylinder, its core component, is vital for the industry's green transformation. Previous researchers have proposed a novel, highly efficient, and energy-saving multi-channel cylinder dryer (MCD) [1]. A series of small rectangular channels are evenly distributed inside the cylinder wall, as shown in **Fig. 1**. The steam could flow inside the channels and heat the cylinder wall. The small rectangular channels could not only increase the heat exchange areas, but also break the condensate ring formed during the steam, releasing heat and being condensed; achieving heat transfer coefficients 7–20 times higher than conventional dryers; and demonstrating significant energy-saving potential [2]. However, under actual operating conditions, each channel rotates about the central axis of the cylinder, as illustrated in Fig. 1. The Coriolis force and centrifugal force generated during rotation fundamentally alter the vapor-liquid interface. This causes steam velocity, flow resistance, and condensation behavior to deviate significantly from static conditions, rendering heat transfer correlations derived under static conditions inadequate for accurate design. While existing research on rotating channel heat transfer has focused primarily on turbine cooling and thermosiphon tubes, investigations into steam condensation characteristics remain scarce. Given that channel spacing is a critical geometric parameter, a thorough exploration of steam condensation mechanisms under rotational conditions is of significant theoretical and engineering value for optimizing MCD structural design and enhancing drying energy efficiency.

Previous studies have elucidated several key factors influencing condensation heat transfer, including mass flux [3-5], channel aspect ratio [6-8], and saturation temperature [9,10]. Wang et al. [11] observed that the aspect ratio of channels positively correlates with the condenser's Nusselt number but negatively correlates with the evaporator's thermal resistance. In contrast, Chiu et al. [12] demonstrated that reducing the aspect ratio enhances the condensation heat

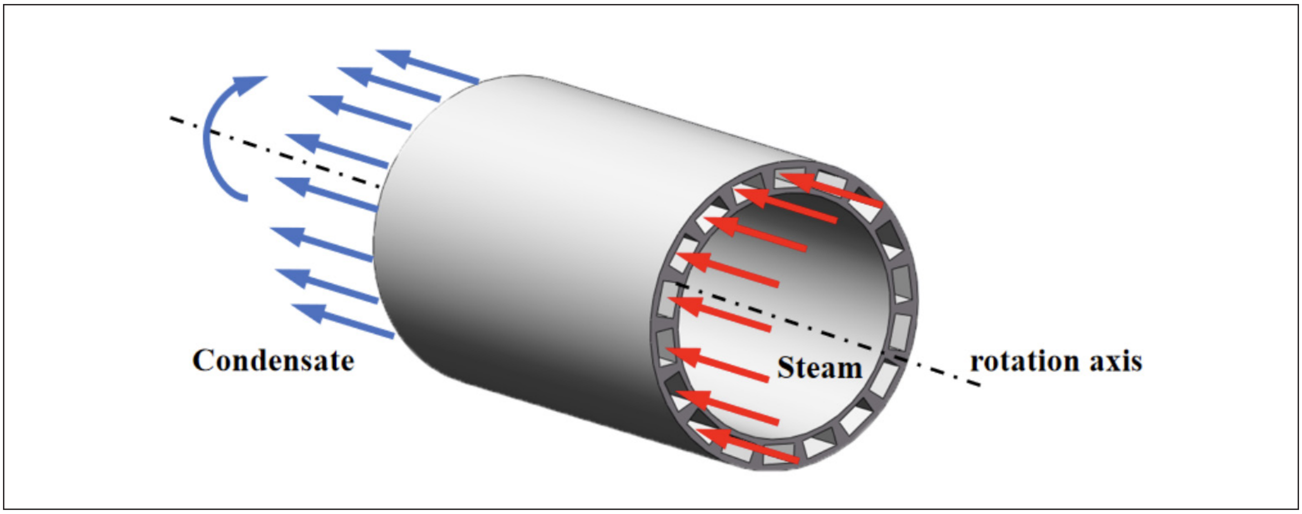

1. Schematic diagram of multi-channel cylinder dryer (MCD).

transfer coefficient; however, they also noted that the associated increase in pressure drop is more pronounced in channels with higher aspect ratios, which in turn further boosts heat transfer performance. Addressing this complexity, Pan et al. [13] found that microchannel heat exchangers exhibit optimal performance at a specific aspect ratio, a value that varies depending on the working fluid and material properties. Expanding on geometric factors, Ahmad et al. [14] showed that certain optimizations, such as increasing the amplitude-to-wavelength ratio or reducing the wavelength-to-fin length ratio, can adversely impact two-phase heat transfer.

Numerical simulations by Pan et al. [13] further confirmed that manifold microchannel heat sinks attain peak efficiency at a specific, fluid- and material-dependent aspect ratio. They reported that this optimal value increases with higher wall thermal conductivity and fluid viscosity, while it decreases with increasing specific heat and thermal conductivity of the working fluid. Beyond aspect ratio, other geometric parameters like spacing are crucial. Li et al. [15] explored how inner tube spacing affects heat storage systems, determining that a 20-mm spacing yielded optimal charging and discharging efficiency. Similarly, Zhang et al. [16], in their study of heat pipe exchangers, recommended using medium tube diameters and minimal spacing to improve performance.

Regarding operational parameters, Sun et al. [17] found that increasing the mass flow rate significantly improves the condensation heat transfer coefficient, with values rising from 28.6 to 45.8 kW/(m^2·K) as the flow rate increased from 0.029 to 0.072 kg/s. These findings were corroborated by Ammar et al. [18,19], who also confirmed the positive effect of an increased mass flow rate. In the context of rotation, Wang et al. [20,21] experimentally showed that higher rotation speeds enhance heat transfer while concurrently reducing pressure drop, and they proposed a new empirical correlation to predict this behavior.

Despite a growing interest in condensation heat transfer within horizontal rotating channels, the influence of channel spacing on steam condensation performance remains insufficiently explored. Moreover, a unified metric that integrates both heat transfer efficiency and flow resistance to provide a comprehensive evaluation of condensation performance is currently lacking. To bridge these critical gaps, the present study introduces a novel dimensionless parameter, grounded in similarity principles, which serves as a comprehensive index reflecting the combined effects of channel spacing and mass flux. Accordingly, a functional relationship for this index is derived, and its response to varying design parameters is systematically analyzed. This aims to provide theoretical foundations and technical guidance for structural optimization and operational parameter selection in MCDs for paper machines.

DESCRIPTION OF EXPERIMENTAL APPARATUS

The test apparatus comprises a steam circulation system and a cooling water circulation system, designed to investigate the condensation heat transfer characteristics of steam in channels during rotation. The cooling water circulation system simulates a wet paper, operating at a flow rate of 200 kg/h and a temperature of 20°C. The entire system employs a rotating mechanism to replicate the operational conditions of an actual drying cylinder. The radius of the rotating device is 400 mm and the length of channel is 1100 mm. The schematic diagram of the experimental apparatus and the site photo of the experimental apparatus are shown in **Fig. 2a** and **Fig. 2b**, respectively.

The experimental section serves as the core region of the entire apparatus, where the primary steam condensing process occurs. Sixteen temperature sensors are installed within the cooling water channel, wall, and steam channel of the experimental test section to directly measure cooling water temperature, wall temperature, and steam tem-

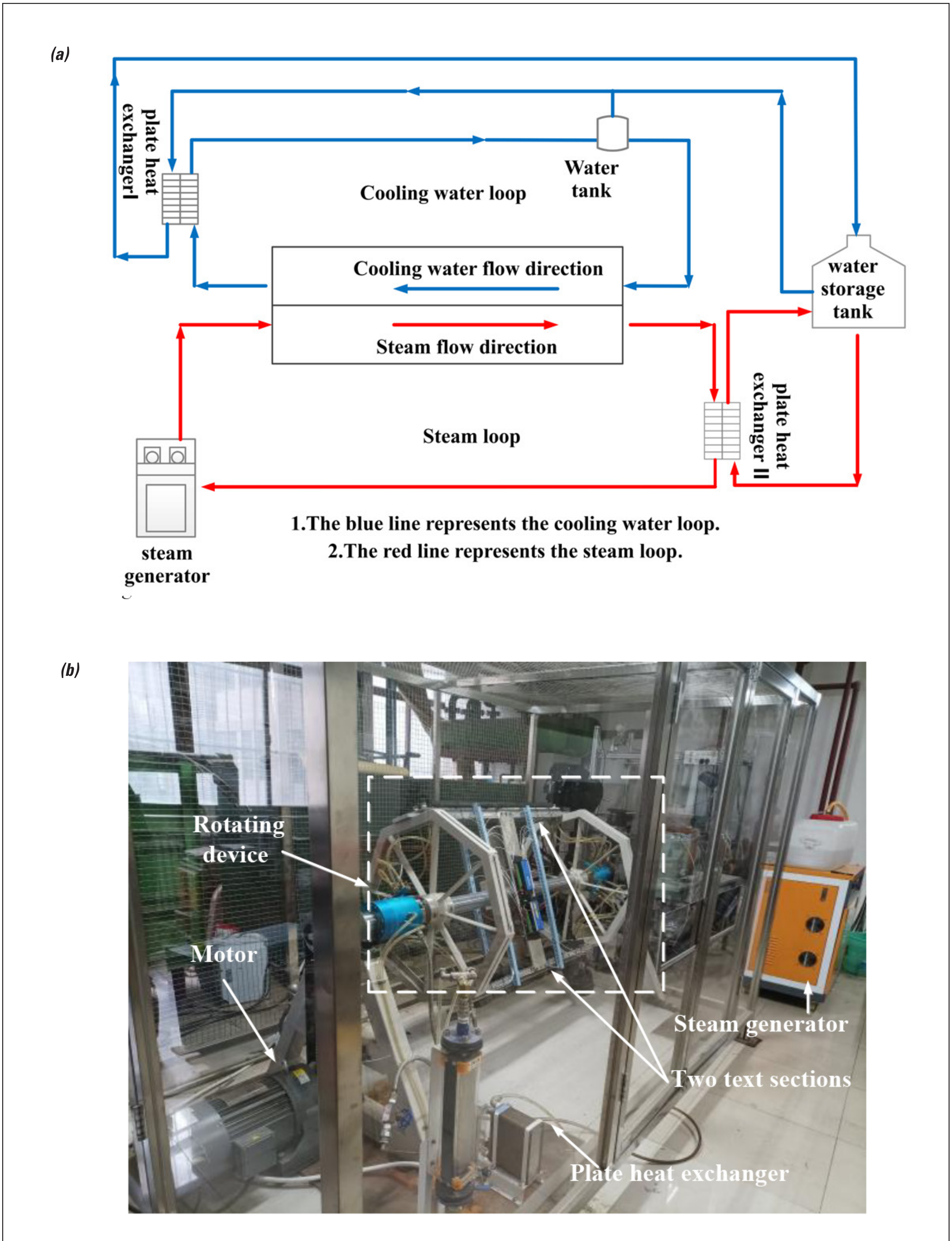

2. (a) Schematic diagram of the experimental apparatus, and (b) site photo of the experimental apparatus.

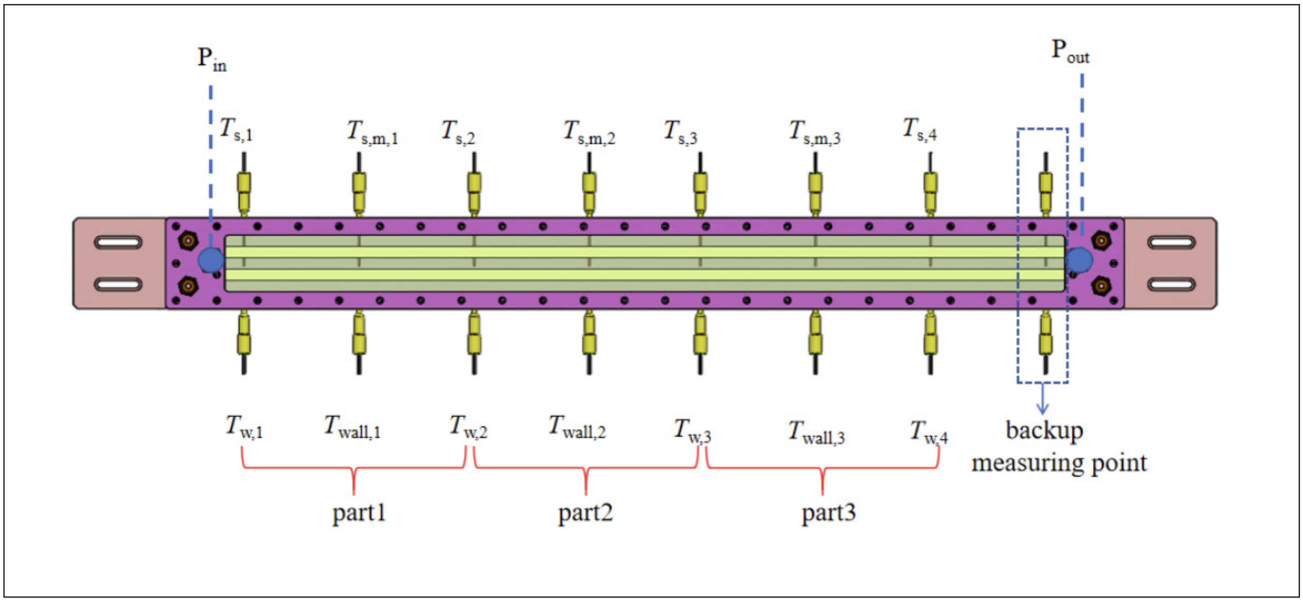

3. Schematic diagram of temperature and pressure distribution measurement points as discussed in the Experimental Apparatus section.

perature. Two pressure sensors are installed at the inlet and outlet of the steam channel in the experimental section to detect inlet and outlet steam pressures. The arrangement of pressure sensors and temperature sensors is shown in **Fig. 3**.

The rotational speed, n, range in this experiment is 50~100 rpm, corresponding to an angular velocity, ω, range of 5.236~10.742 rad/s. The steam mass flow rate G is set within the range of 50~80 kg/(m^2·s). Some scholars have demonstrated that channels with an aspect ratio, r_{HW}, of 1:3 exhibit optimal heat transfer performance in static conditions. Based on this, the experimental channel aspect ratio is set within the range of 1:2 to 1:4.

Since the entire experimental section was almost thermally insulated, heat loss to the environment during heat exchange was less than 5%. Therefore, the heat loss from the experimental section can be neglected. The heat released by the steam equals the heat absorbed by the cooling water:

$$Q_{s,i} = Q_{w,i} \tag{1}$$

where:

$Q_{s,i}$: heat released by each portion of steam (J)

$Q_{w,i}$: heat absorbed by each portion of cooling water (J)

The formula for calculating the heat absorbed by the cooling water is:

$$Q_{w,i} = c_p m_w (T_{w,i+1} - T_{w,i}) \tag{2}$$

where:

c_p: specific heat capacity of cooling water (J·kg^{-1}·K^{-1})

m_w: mass flow rate of cooling water (kg·s^{-1})

$T_{w,i}$ and $T_{w,i+1}$: inlet and outlet temperatures of each section of cooling water (°C)

The heat released by steam in each section is given by:

$$Q_{s,i} = A_{c,i} h_i (T_{s,m,i} - T_{wall,i}) \tag{3}$$

where:

$A_{c,}$: heat transfer area of each test section (m^2)

h_i: heat transfer coefficient for steam condensation in each section (W·m^{-2}·K^{-1})

$T_{s,m,i}$: steam temperature of each section (°C)

$T_{wall,i}$: wall temperature (°C) of each section

The local condensation heat transfer coefficient in the channel is calculated as follows:

$$h_i = \frac{Q_{s,i}}{A_{c,i}(T_{s,m,i} - T_{wall,i})} \tag{4}$$

The total pressure drop is calculated by the difference between the two pressure sensors, which comprises these components: the gravitation pressure drop (ΔP_{gr}); the acceleration pressure drop (ΔP_{ac}); *friction* pressure drop (ΔP); and local pressure drop due to inlet sudden contraction (ΔP_{in}) and outlet sudden expansion (ΔP_{out}). The friction pressure drop ΔP is used as the pressure drop parameter for subsequent analysis. Since the channel remains horizontal throughout with no elevation difference between inlet and outlet, gravitation pressure drop is disregarded. The pressure drop caused by the combined effects of centrifugal force and gravity is calculated as acceleration pressure drop. The calculation of each component pressure drop is shown in Eq. 5.

$$\Delta P_{tp} = \Delta P_{gr} + \Delta P_{ac} + \Delta P + \Delta P_{in} + \Delta P_{out} \quad (5)$$

$$\Delta P_{ac} = \rho_{tp}\left[\frac{d\vec{\omega}}{dt}\times\vec{r} + \vec{\omega}\times(\vec{\omega}\times\vec{r}) + 2\vec{\omega}\times\vec{V}_r + \vec{g}_c\right] \quad (6)$$

$$\Delta P_{in} = \left[\frac{G^2(1-\sigma_1)}{\sigma_1^2}\right]\left\{\begin{array}{l}\dfrac{1+\sigma_1}{2\left(\dfrac{x}{\rho_v}+\dfrac{1-x}{\rho_l}\right)}\left[\dfrac{x^3}{\rho_v^2\alpha^2}+\dfrac{(1-x)^3}{\rho_l^2(1-\alpha)^2}\right] \\ -\sigma_1\left[\dfrac{x^2}{\rho_v\alpha}+\dfrac{(1-x)^2}{\rho_l(1-\alpha)}\right]\end{array}\right\} \quad (7)$$

$$\Delta P_{out} = -\frac{G^2(1-\sigma_2^2)\left[\dfrac{x^3}{\rho_v^2\alpha^2}+\dfrac{(1-x)^3}{\rho_l^2(1-\alpha)^2}\right]}{2\left(\dfrac{x}{\rho_v}+\dfrac{1-x}{\rho_l}\right)} + \frac{G^2\sigma(1-\sigma)}{\rho_l}\left[\frac{(1-x)^2}{(1-\alpha)}+\left(\frac{\rho_l}{\rho_v}\right)\frac{x^2}{\alpha}\right] \quad (8)$$

where:

r: relative position of the fluid (mm)
$V_{(r)}$: relative velocity of the fluid (m/s)
g_c: gravitational acceleration vector
G: steam mass flux (kg·m^{-2}·s^{-1})
ρ_v: saturated steam density (kg/m^3)
ρ: saturated water density (kg/m^3)
x: steam dryness (%)
σ_1: ratio of connecting pipe cross-sectional area to inlet cross-sectional area
α: gas content fraction (%)
σ_2: ratio of connecting pipe cross-sectional area to outlet cross-sectional area

The measurement instruments and their accuracies used in this experiment are shown in **Table I**.

The uncertainty calculation formula is as follows, with the uncertainties of each parameter shown in **Table II**.

$$\sigma R = \sqrt{\left(\frac{\partial f}{\partial x_1}\right)^2\delta x_1 + \left(\frac{\partial f}{\partial x_2}\right)^2\delta x_2 + \left(\frac{\partial f}{\partial x_3}\right)^2\delta x_3 + \cdots + \left(\frac{\partial f}{\partial x_n}\right)^2\delta x_n} \quad (9)$$

To validate the measurement accuracy of the experimental section and the reliability of the test apparatus, con-

Measurement Instrument	Model	Accuracy
Temperature sensor	PT100	±0.25%
Pressure transmitter	PCM300	±0.5%
Turbine flow meter	Omega-FLR1009-BR-D	±1%
Glass rotameter	LZB-25	1.5%

I. Experimental instruments and accuracy.

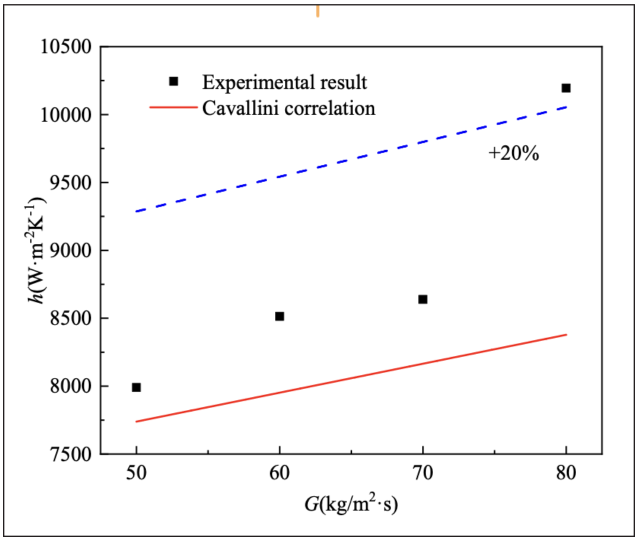

4. Comparison of experimental results with Cavallini correlation.

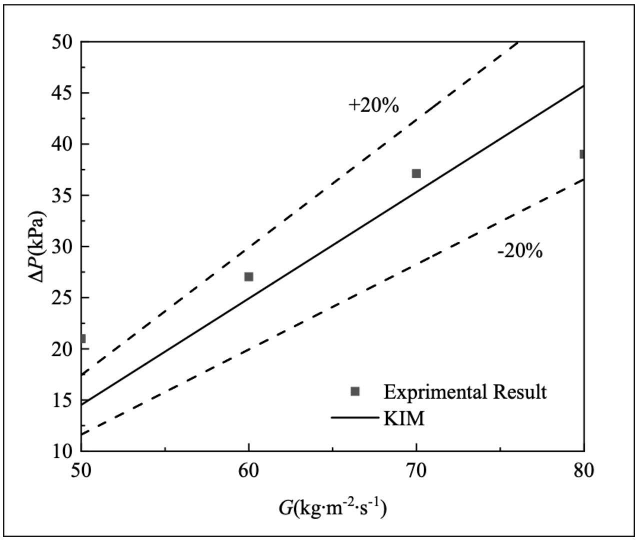

5. Comparison of experimental result with KIM correlation for rectangular channel.

Parameter	Uncertainty
Steam Temperature, °C	±0.77%
Cooling water temperature, °C	±0.77%
Wall temperature, °C	±0.77%
Steam flux, kg/(m^2·s)	±0.95%
Steam dryness	±9.51%
Condensation heat transfer coefficient, W/(m^2·K)	±7.65%
Nusselt number	±13.97%
Pressure drop, kPa	±3.6%

II. Uncertainty of each parameter.

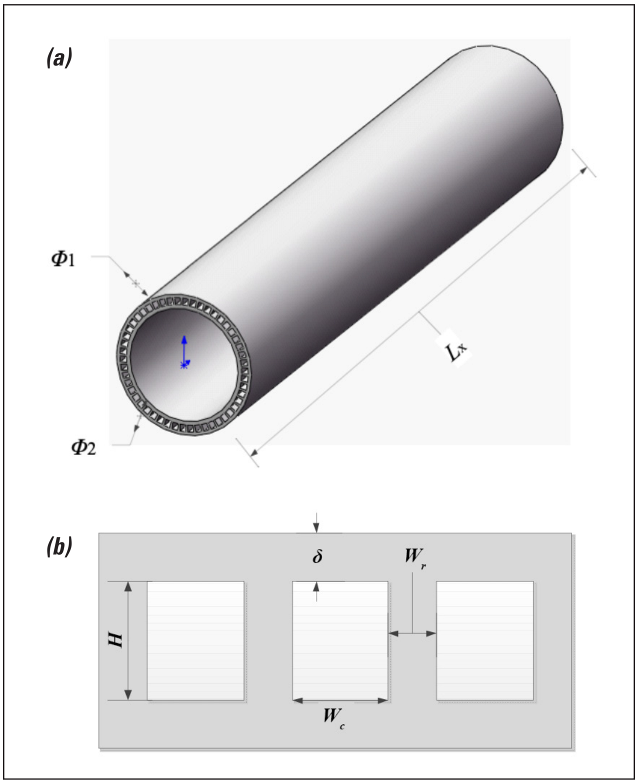

6. (a) Schematic diagram of the dimensions of the multi-channel dryer, and (b) enlarged view of channel structure.

densation heat transfer and pressure drop experiments were conducted in a stationary channel [22,23]. The comparison results are shown in **Fig. 4** and **Fig. 5**. As seen in the figures, most data errors are within 20%, indicating that the reliability of the test apparatus meets the requirements.

MODEL DEVELOPMENT

The dryer unit under investigation is modeled as a cylindrical shell with an outer diameter (Φ_1) of 800 mm and an axial length (L_x) of 1100 mm, as depicted in **Fig. 6a**. Uniformly embedded within the cylindrical surface is an array of narrow rectangular channels, each defined by a width W_c and height H. These channels form a series of parallel passages designed for steam flow and condensation, as shown schematically in Fig. 6b.

Due to the curvature of the cylindrical shell, a slight geometric asymmetry exists in the spacing between adjacent channels, where the upper gap (W_{r1}) differs from the lower gap (W_{r2}). However, since the inner diameter of the shell Φ_2 is significantly larger than the individual channel dimensions, this distortion is considered negligible. Therefore, to simplify the model without compromising accuracy, a uniform spacing is assumed, where W_{r1}=W_{r2}=W_r. This value, W_{r1}, is adopted as the average inter-channel spacing for all subsequent analyses.

The overall performance of steam condensation within a horizontally rotating channel is primarily governed by two key parameters: steam mass flux and inter-channel spacing. Effective optimization of these parameters is crucial for maximizing heat transfer while simultaneously minimizing the associated pressure losses. However, existing studies typically evaluate these effects in isolation, focusing on either the condensation heat transfer coefficient or the pressure drop. A unified criterion that accounts for both factors concurrently is conspicuously absent. This gap underscores the need for a comprehensive performance metric capable of evaluating the system's overall efficiency by integrating its thermal and hydraulic characteristics.

In the MCD, the role of inter-channel spacing is particularly critical. Heat exchange occurs not only through the channel walls but also via lateral conduction across adjacent channels, a mechanism in which the spacing plays a non-negligible role. Furthermore, for a given rotation radius, the number of channels is geometrically coupled with the channel spacing. Consequently, this single geometric parameter simultaneously influences both the total available heat transfer area and the system pressure drop. Therefore, to properly account for these coupled effects, this study proposes a novel dimensionless evaluation index based on similarity theory. This new index is designed to replace the conventional single-channel Nusselt number, as it holistically captures the combined influence of mass flux and channel spacing and serves as a comprehensive descriptor of the thermo-hydraulic performance in rotating channels.

The macroscopic motion of a fluid, fundamentally governed by Newton's second law, adheres to the principles of mechanical similarity. This foundation enables the use of pressure-based similarity analysis to characterize flows with analogous pressure dynamics. The central criterion in this analysis is the Euler number (*Eu*), which defines the ratio of pressure forces acting on a fluid element. It is expressed as:

$$\frac{P}{\rho v^2} = Eu \tag{10}$$

where:

P: fluid pressure (Pa)
ρ: fluid density (kg/m³)
v: fluid velocity (m/s)

The pressure similarity criterion dictates that fluid elements are subjected to dynamically equivalent pressure effects when their respective Euler numbers are identical. Consequently, by utilizing the pressure differential (ΔP) in its formulation, the Euler number is adopted in this study as the characteristic descriptor for flow-induced pressure drop.

For the thermal aspect of the analysis, the governing heat transfer relationship is expressed as:

$$\begin{cases} Q=kA\Delta T \\ q=k\Delta T \end{cases} \tag{11}$$

where:

k: overall heat transfer coefficient (W·m^{-2}·K^{-1})

Based on Fourier's law of heat conduction, which establishes the fundamental relationship between heat transfer and temperature gradients, the local heat flux is given by:

$$q=-\lambda\left.\frac{\partial T}{\partial x}\right|_{x=x_i} \tag{12}$$

where:
x_i: heat exchanger wall position coordinates.

$\left.\frac{\partial T}{\partial x}\right|_{x=x_i}$: change rate of fluid temperature in the direction normal to the heat exchanger wall surface.

Under the principle of energy conservation at the interface, the net heat transferred must equal the heat conducted through the adjacent wall boundary layer. Therefore, combining the expressions in Eq. 11 and Eq. 12 yields the following relationship:

$$k=-\frac{\lambda'}{\Delta T}\left.\frac{\partial T}{\partial x}\right|_{x=x_i} \tag{13}$$

where:
λ: integrated thermal conductivity of wall and liquid

Suppose two independent heat transfer processes exhibit geometric and physical similarity:

$$k_A=-\frac{\lambda'_A}{\Delta T_A}\left.\frac{\partial T_A}{\partial x_A}\right|_{x=xi} \qquad k_B=-\frac{\lambda'_B}{\Delta T_B}\left.\frac{\partial T_B}{\partial x_B}\right|_{x=x_j} \tag{14}$$

Following the principle of similarity, a direct proportionality must exist between the corresponding physical parameters of the two systems. This relationship is expressed as:

$$\begin{cases}\dfrac{k_A}{k_B}=C_k\\ \dfrac{\lambda'_A}{\lambda'_B}=C_{\lambda'}\\ \dfrac{T_A}{T_B}=C_T\\ \dfrac{x_A}{x_B}=C_l\end{cases} \tag{15}$$

Substituting Eq. 15 into Eq. 14 gives:

$$\frac{C_k C_l}{C_{\lambda'}}k_B=-\frac{\lambda'_B}{\Delta T_B}\frac{\partial T_B}{\partial x_B} \tag{16}$$

Comparing Eq. 14 and Eq. 16, it can be obtained:

$$\frac{C_k C_l}{C_{\lambda'}}=1 \tag{17}$$

Since the left side of Eq. 17 equals a constant, it has:

$$\frac{C_{k,A}C_{l,A}}{C_{\lambda',A}}=\frac{C_{k,B}C_{l,B}}{C_{\lambda',B}} \tag{18}$$

Substituting Eq. 15 into Eq. 17, gives:

$$\frac{k_A x_A}{\lambda'_A}=\frac{k_B x_B}{\lambda'_B} \tag{19}$$

That is:

$$\left(\frac{kD_h}{\lambda'}\right)_1=\left(\frac{kD_h}{\lambda'}\right)_2 \tag{20}$$

A new dimensionless number, W, is therefore introduced to holistically characterize the variation in total heat transfer performance within horizontally rotating channels, defined as:

$$W=\frac{kD_h}{\lambda'} \tag{21}$$

$$k=\frac{1}{\dfrac{A_{s1}+A_{s2}}{\lambda\left(\dfrac{A_{s1}}{\delta}+\dfrac{A_{s2}}{\delta+H\eta_f}\right)}+\dfrac{1}{h_c}} \tag{22}$$

$$\lambda'=\frac{2}{\dfrac{1}{\lambda_{wall}}+\dfrac{1}{\lambda_{liq}}} \tag{23}$$

$$D_h=\frac{2Hw_c}{H+w_c} \tag{24}$$

$$A_{s1}=NW_cL_x \tag{25}$$

$$A_{s2}=N\frac{(W_r+2H\eta_f)}{2}L_x \tag{26}$$

where:
λ_{wall}: thermal conductivity of the wall ($W\cdot m^{-2}\cdot K^{-1}$).
λ_{liq}: thermal conductivity of the fluid ($W\cdot m^{-2}\cdot K^{-1}$)
D_h: hydraulic diameter of the channel (m)
A_{s1}: area of heat exchange through the main wall of the cylinder (m^2)
A_{s2}: area of heat transfer through the channel's side wall (m^2)
η_f: efficiency factor of side-wall heat transfer. Given the analogy between side-wall ehancement and rib-augmented heat transfer, the efficiency is approximated using a rectangular rib model, with $\eta_f = 0.6$.
N: number of rectangular channels inside the cylinder.

By integrating the preceding thermal and hydraulic analyses, it can be seen that W represents the dimensionless value of the heat transfer coefficient within the channel, while Eu represents the dimensionless value of the pressure drop within the channel. To maximize the heat transfer coefficient and minimize the flow pressure drop within the channel, this study proposes the ratio *W/Eu* as a unified, dimensionless performance index. This index is designed to holistically evaluate the system by simultaneously accounting for both condensation heat transfer and flow resistance characteristics within the rotating channel.

RESULTS AND DISCUSSION

Figure 7 illustrates the comprehensive thermo-hydraulic performance index, *W/Eu*, as a function of key operational

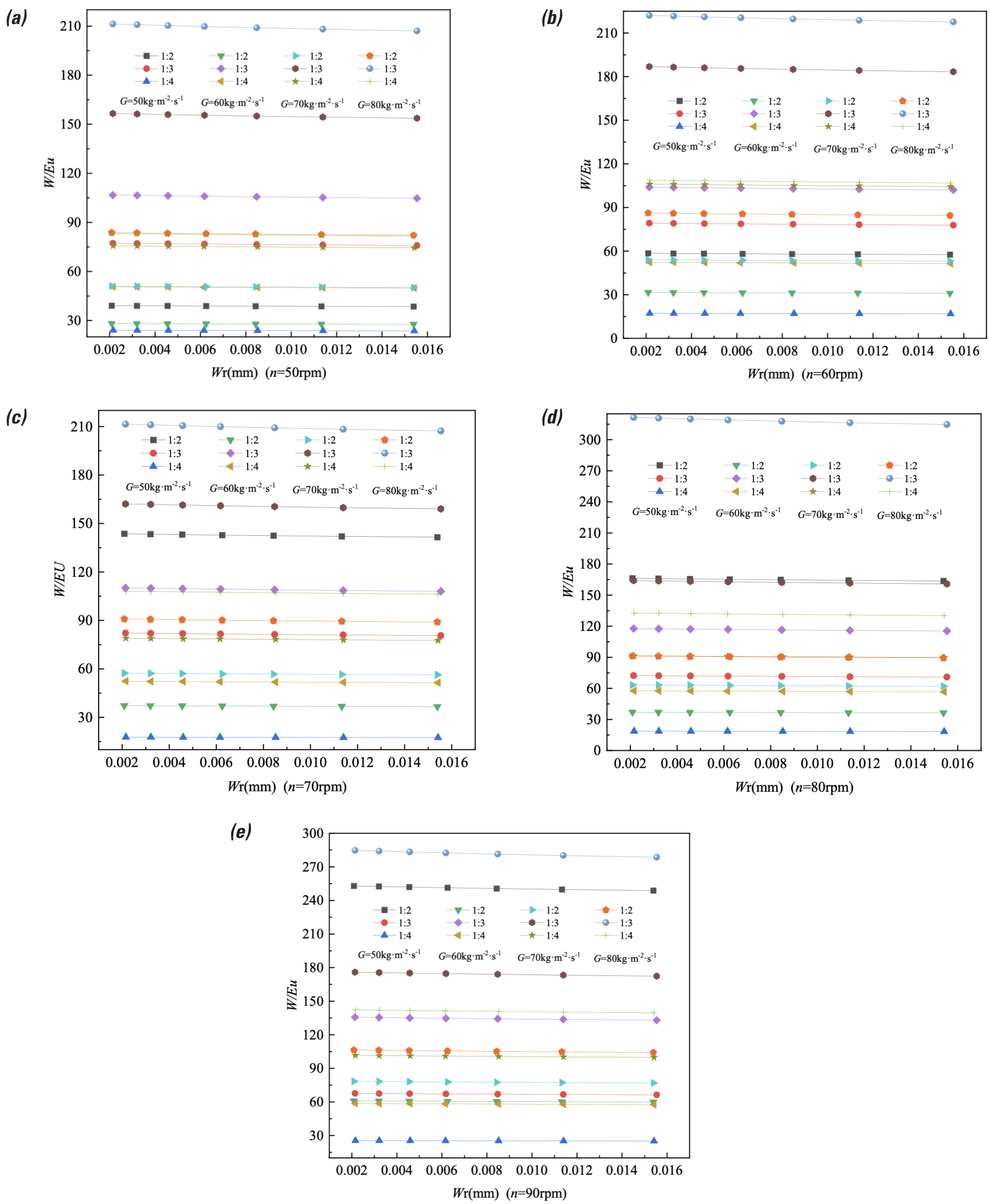

7. Variation of W/Eu *under different mass flux: (a) 50 rpm; (b): 60 rpm); (c): 70 rpm; (d): 80 rpm; and (e) 90 rpm.*

parameters. A consistent observation across all rotating speeds is that the 1:4 aspect ratio channel yields the lowest *W/Eu* value (specifically at a mass flux of 50 $kg{\cdot}m^{-2}{\cdot}s^{-1}$), whereas the 1:3 channel achieves the highest *W/Eu* value (at a mass flux of 80 $kg{\cdot}m^{-2}{\cdot}s^{-1}$). This can be explained by the trade-off between heat transfer and pressure drop, as detailed in a previous study [24]. The 1:4 channel exhibits the highest heat transfer coefficient but suffers from a disproportionately large pressure drop. In contrast, the 1:3 channel provides a heat transfer coefficient nearly as high but with significantly lower flow resistance. The 1:2 channel shows moderate performance in both aspects. Consequently, according to the definition of *W/Eu*, the 1:3 channel, with its more favorable balance of relatively high heat transfer and lower pressure drop, demonstrates a superior overall performance index.

The influence of rotational speed on the 1:3 channel's performance is most notable at a low mass flux ($G = 50$ $kg{\cdot}m^{-2}{\cdot}s^{-1}$), where *W/Eu* first increases and then decreases, though the overall variation is not significant. This trend directly mirrors the behavior of its heat transfer coefficient, which follows the same non-monotonic pattern with increasing rotational speed, while its pressure drop decreases monotonically [24]. As *W/Eu* represents the ratio of these two competing factors, its resulting trend is non-monotonic.

For the 1:2 aspect ratio channel, the *W/Eu* index increases substantially with rotational speed at a mass flux of 50 $kg{\cdot}m^{-2}{\cdot}s^{-1}$; however, this increase is much more gradual at higher mass fluxes. The significant rise at $G = 50$ is attributed to the pressure drop diminishing to a very low level at high rotating speeds while the heat transfer coefficient increases monotonically [20]. This combination of a rapidly falling denominator and a rising numerator causes the marked increase in *W/Eu*. At other mass fluxes, although the pressure drop also decreases monotonically with speed, its magnitude remains larger compared to the G=50 case. Since the heat transfer coefficients do not differ substantially across the various mass fluxes, the growth of *W/Eu* in these other cases is less pronounced.

The performance of the 1:4 aspect ratio channel shows a strong dependence on mass flux. At low mass fluxes, *W/Eu* remains largely insensitive to changes in rotational speed. This is because the heat transfer coefficient exhibits a slight non-monotonic trend while the pressure drop, though decreasing, changes by a smaller magnitude compared to its behavior at high mass fluxes [24]. As a result, *W/Eu* fluctuates within a very narrow range. As the mass flux increases to 70 and then 80 $kg{\cdot}m^{-2}{\cdot}s^{-1}$, the pressure drop at low rotating speeds becomes much more significant. Consequently, as the rotational speed increases, the resulting reduction in pressure drop causes the *W/Eu* index to exhibit a more pronounced fluctuating trend or a significant monotonic increase.

A consistent, though minor, trend observed in all experimental cases is the slight decrease in *W/Eu* with an increase in channel spacing, W_r. This phenomenon occurs because an increase in W_r elevates the channel's thermal resistance, which in turn slightly reduces the heat transfer coefficient. Since variations in W_r do not affect the pressure drop, the *W/Eu* index shows a marginal, monotonically decreasing trend driven solely by the change in thermal performance.

In this section, a qualitative analysis of the variation of *W/Eu* with channel aspect ratio, mass flux, rotational speed, and channel spacing has been conducted. To achieve a complete optimization of the flow and heat transfer within the channel, a rigorous quantitative analysis is necessary.

ANALYSIS AND OPTIMIZATION OF COMPREHENSIVE EVALUATION INDEX

This section will focus on constructing a mathematical model that expresses the relationship between *W/Eu* and mass flux channel spacing. Then a first-order optimization analysis to obtain a specific, optimal design scheme is subjected.

Functional formulation of comprehensive evaluation index

Based on the preceding definitions of the Euler number (*Eu*) and the dimensionless parameter *W*, the comprehensive performance indicator, *W/Eu*, is formulated as the ratio of these two quantities:

$$\frac{W}{Eu} = \frac{kD_{\mathrm{h}}\rho v^2}{\lambda' P} \tag{27}$$

r_{HW} is the ratio of channel height *H* to channel width *W*, and it is defined as follows:

$$r_{HW} = \frac{H}{W_{\mathrm{c}}} \tag{28}$$

Then, the hydraulic diameter D_{h} can be expressed as:

$$D_{\mathrm{h}} = \frac{2H^2}{r_{HW}(H + \dfrac{H}{r_{HW}})} = \frac{2H^2}{r_{HW}H + H} = \frac{2H}{1 + r_{HW}} \tag{29}$$

Drawing upon established empirical models from previous studies [20,21], the condensation heat transfer coefficient, h_c, and pressure drop, ΔP, within a single channel can be approximated by the following functional forms:

$$P = P(Re_{lo}, Re_{\omega}) = f_P(G, \omega) \tag{30}$$

$$h_{\mathrm{c}} = \frac{Nu(Re, Re_{\omega})D_{\mathrm{h}}}{\lambda_{\mathrm{liq}}} = f_h(G, \omega) \tag{31}$$

Additionally, it is known that:

$$v = \frac{G}{\rho} \tag{32}$$

where:

G: steam mass flux ($\mathrm{kg \cdot m^{-2} \cdot s^{-1}}$)

By substituting Eq. 13 and Eq. 32 into Eq. 27, the expression for *W/Eu* becomes:

$$\begin{aligned}
\frac{W}{Eu} &= \frac{kD_{\mathrm{h}}\rho v^2}{\lambda' P} \\
&= \frac{H\lambda_{\mathrm{wall}}}{\rho}\left(\frac{1}{\lambda_{\mathrm{wall}}}+\frac{1}{\lambda_{\mathrm{liq}}}\right)\frac{\frac{2H}{\delta}G^2h_{\mathrm{c}}+\frac{1}{\delta+H\eta_{\mathrm{f}}}r_{HW}G^2h_{\mathrm{c}}W_{\mathrm{r}}+\frac{2H\eta_{\mathrm{f}}}{\delta+H\eta_{\mathrm{f}}}r_{HW}G^2h_{\mathrm{c}}}{P\left(\begin{array}{l} 2Hh_{\mathrm{c}}+2Hh_{\mathrm{c}}r_{HW}+W_{\mathrm{r}}h_{\mathrm{c}}r_{HW}+W_{\mathrm{r}}h_{\mathrm{c}}r_{HW}^2+2H\eta_{\mathrm{f}}h_{\mathrm{c}}r_{HW}+ \\ 2H\eta_{\mathrm{f}}h_{\mathrm{c}}r_{HW}^2+\frac{2H\lambda_{\mathrm{wall}}}{\delta}+\frac{2H\lambda_{\mathrm{wall}}}{\delta}r_{HW}+\frac{\lambda_{\mathrm{wall}}}{\delta+H\eta_{\mathrm{f}}}W_{r}r_{HW}+ \\ \frac{\lambda_{\mathrm{wall}}}{\delta+H\eta_{\mathrm{f}}}W_{\mathrm{r}}r_{HW}^2+\frac{2H\eta_{\mathrm{f}}+\lambda_{\mathrm{wall}}}{\delta+H\eta_{\mathrm{f}}}r_{HW}+\frac{2H\eta_{\mathrm{f}}+\lambda_{\mathrm{wall}}}{\delta+H\eta_{\mathrm{f}}}r_{HW}^2 \end{array}\right)} \\
&= A_0\frac{A_1G^2f_{\mathrm{h}}(G,\omega)+A_2r_{HW}G^2W_{\mathrm{r}}f_{\mathrm{h}}(G,\omega)+A_3r_{HW}G^2f_{\mathrm{h}}(G,\omega)}{f_P(G,\omega)\left(\begin{array}{l} A_4f_{\mathrm{h}}(G,\omega)+A_5r_{HW}f_{\mathrm{h}}(G,\omega)+W_{\mathrm{r}}r_{HW}f_h(G,\omega)+W_{\mathrm{r}}r_{HW}^2f_{\mathrm{h}}(G,\omega)+ \\ A_6r_{HW}^2f_{\mathrm{h}}(G,\omega)+A_7+A_8W_{\mathrm{r}}r_{HW}+A_8W_{\mathrm{r}}r_{HW}^2+A_9r_{HW}^2 \end{array}\right)}
\end{aligned} \tag{33}$$

where:

$A_0 - A_9$: composite coefficients independent of G and W_{r}

$$\begin{aligned}
A_0 &= \frac{H\lambda_{\mathrm{wall}}}{\rho}\left(\frac{1}{\lambda_{\mathrm{wall}}}+\frac{1}{\lambda_{\mathrm{liq}}}\right) \\
A_1 &= \frac{2H}{\delta} \\
A_2 &= \frac{1}{\delta+H\eta_{\mathrm{f}}} \\
A_3 &= \frac{2H\eta_{\mathrm{f}}}{\delta+H\eta_{\mathrm{f}}} \\
A_4 &= 2H \\
A_5 &= 2H(1+\eta_{\mathrm{f}}) \\
A_6 &= 2H\eta_{\mathrm{f}} \\
A_7 &= \frac{2H\lambda_{\mathrm{wall}}}{\delta} \\
A_8 &= \frac{\lambda_{\mathrm{wall}}}{\delta+H\eta_{\mathrm{f}}} \\
A_9 &= \frac{2H\eta_{\mathrm{f}}\lambda_{wall}}{\delta+H\eta_{\mathrm{f}}}
\end{aligned} \tag{34}$$

Analysis and optimization based on first-order optimization process

To examine the response of the comprehensive evaluation index, *W/Eu*, to variations in channel spacing (W_{r}) and steam mass flux (G), a first-order optimization process was performed. This approach involves deriving the partial derivatives of the index with respect to each parameter, which facilitates the identification of theoretical maxima.

For the analysis of the channel spacing's effect, W_{r} is treated as the sole independent variable while all other parameters are held constant. Under these conditions, the simplified functional form of the index is:

$$\begin{aligned}
\frac{W}{Eu} &= A_0\frac{A_1G^2f_h(G,\omega)+A_2r_{HW}G^2W_{\mathrm{r}}f_h(G,\omega)+A_3r_{HW}G^2f_h(G,\omega)}{f_P(G,\omega)\left(\begin{array}{l} A_4f_h(G,\omega)+A_5r_{HW}f_h(G,\omega)+W_{\mathrm{r}}r_{HW}f_h(G,\omega)+ \\ W_{\mathrm{r}}r_{HW}^2f_h(G,\omega)+A_6r_{HW}^2f_h(G,\omega)+A_7+A_8W_{\mathrm{r}}r_{HW}+ \\ A_8W_{\mathrm{r}}r_{HW}^2+A_9r_{HW}^2 \end{array}\right)} \\
&= B_0\frac{B_1+B_2W_{\mathrm{r}}}{B_3+B_4W_{\mathrm{r}}}
\end{aligned} \tag{35}$$

where:

$$\begin{aligned}
B_0 &= \frac{A_0}{f_P(G,\omega)} \\
B_1 &= A_1G^2f_h(G,\omega)+A_3r_{HW}G^2f_h(G,\omega) \\
B_2 &= A_2r_{HW}G^2f_h(G,\omega) \\
B_3 &= A_4f_h(G,\omega)+A_5r_{HW}f_h(G,\omega)+A_6r_{HW}^2f_h(G,\omega)+A_7+A_9r_{HW}^2 \\
B_4 &= r_{HW}f_h(G,\omega)+r_{HW}^2f_h(G,\omega)+A_8r_{HW}+A_8r_{HW}^2
\end{aligned} \tag{36}$$

A partial derivative function for W_{r} is obtained:

$$\frac{\partial\left(\frac{W}{Eu}\right)}{\partial W_{\mathrm{r}}} = B_0\frac{B_2B_3-B_1B_4}{\left(B_3+B_4W_{\mathrm{r}}\right)^2} \tag{37}$$

Since all system constants and physical properties involved are positive, coefficients $A_0 - A_9$ and $B_0 - B_4$ are all strictly positive. Because the denominator of Eq. 36 remains positive, the numerator for all $W_{\mathrm{r}}>0$ is:

$$\begin{aligned}
&B_2B_3-B_1B_4 \\
&= -\frac{2H\lambda_{\mathrm{wall}}(\delta+H\eta_{\mathrm{f}}+\delta\eta_{\mathrm{f}})}{\delta(\delta+H\eta_{\mathrm{f}})^2}r_{HW}^2-\frac{2H^2\eta_{\mathrm{f}}}{\delta(\delta+H\eta_{\mathrm{f}})}\left(r_{HW}^2f_h(G,\omega)+r_{HW}f_h(G,\omega)\right) \\
&= -\frac{2H}{\delta(\delta+H\eta_{\mathrm{f}})}r_{HW}\left[\begin{array}{l} \lambda_{\mathrm{wall}}(\delta+H\eta_{\mathrm{f}}+\delta\eta_{\mathrm{f}})r_{HW}+ \\ H\eta_{\mathrm{f}}r_{HW}f_h(G,\omega)+H\eta_{\mathrm{f}}f_h(G,\omega) \end{array}\right]<0
\end{aligned} \tag{38}$$

Thus, the partial derivative, $\frac{\partial\left(\frac{W}{Eu}\right)}{\partial W_{\mathrm{r}}}$, is always less than zero for any $W_{\mathrm{r}}>0$. This result indicates that the function *W/Eu* decreases monotonically with respect to W_{r}. Consequently, its theoretical maximum is attained as W_{r} approaches zero ($W_{\mathrm{r}}\to 0$).

$$\begin{aligned}
\left(\frac{W}{Eu}\right)_{W_{\mathrm{r}},\max}\Bigg|_{\substack{G=Const \\ \omega=Const}} &= \lim_{W_{\mathrm{r}}\to 0}B_0\frac{B_1+B_2W_{\mathrm{r}}}{B_3+B_4W_{\mathrm{r}}} = B_0\frac{B_1}{B_3} \\
&= \frac{A_0\left(A_1G^2f_h(G,\omega)+A_3r_{HW}G^2f_h(G,\omega)\right)}{f_P(G,\omega)\left(\begin{array}{l} A_4f_h(G,\omega)+A_5r_{HW}f_h(G,\omega)+ \\ A_6r_{HW}^2f_h(G,\omega)+A_7+A_9r_{HW}^2 \end{array}\right)}
\end{aligned} \tag{39}$$

Similarly, when analyzing the influence of the mass flux, G, it is treated as the sole independent variable while all other parameters are held constant. In this case, Eq. 39 can be simplified to the following form:

$$\begin{aligned}
\frac{W}{Eu} &= A_0\frac{\left(A_1+A_2r_{HW}W_{\mathrm{r}}+A_3r_{HW}\right)G^2f_h(G)\big|_{\omega=Const}}{f_P(G)\big|_{\omega=Const}\left[\begin{array}{l} \left(A_4+A_5r_{HW}+W_{\mathrm{r}}r_{HW}+W_{\mathrm{r}}r_{HW}^2+A_6r_{HW}^2\right)f_h(G)\big|_{\omega=Const}+ \\ \left(A_7+A_8W_{\mathrm{r}}r_{HW}+A_8W_{\mathrm{r}}r_{HW}^2+A_9r_{HW}^2\right) \end{array}\right]} \\
&= \frac{C_1G^2f_h(G)\big|_{\omega=Const}}{f_P(G)\big|_{\omega=Const}\left[C_2f_h(G)\big|_{\omega=Const}+C_3\right]}
\end{aligned} \tag{40}$$

where:

$$
\begin{aligned}
C_1 &= A_0\left(A_1 + A_2 r_{HW} W_{\mathrm{r}} + A_3 r_{HW}\right)\\
C_2 &= A_4 + A_5 r_{HW} + W_{\mathrm{r}} r_{HW} + W_{\mathrm{r}} r_{HW}{}^2 + A_6 r_{HW}{}^2\\
C_3 &= A_7 + A_8 W_{\mathrm{r}} r_{HW} + A_8 W_{\mathrm{r}} r_{HW}{}^2 + A_9 r_{HW}{}^2
\end{aligned}
\tag{41}
$$

A partial derivative function for G is obtained:

$$
\frac{\partial\left(\frac{W}{Eu}\right)}{\partial G} = \frac{\begin{array}{l}\left(2C_1 G\, f_h(G)\big|_{\omega=Const} + C_1 G^2 \frac{\partial f_h(G)}{\partial G}\Big|_{\omega=Const}\right) f_P(G)\Big|_{\omega=Const}\left(C_2\, f_h(G)\big|_{\omega=Const} + C_3\right) - \\ C_1 G^2\, f_h(G)\big|_{\omega=Const} \frac{\partial f_P(G)}{\partial G}\Big|_{\omega=Const}\left(C_2\, f_h(G)\big|_{\omega=Const} + C_3\right) - \\ C_1 G^2\, f_h(G)\big|_{\omega=Const}\, f_P(G)\big|_{\omega=Const}\, C_2 \frac{\partial f_h(G)}{\partial G}\Big|_{\omega=Const}\end{array}}{\left(f_P(G)\big|_{\omega=Const}\right)^2\left[C_2\, f_h(G)\big|_{\omega=Const} + C_3\right]^2}
\tag{42}
$$

It is evident that the denominator of Eq. 42 is always positive. The analysis therefore focuses on the numerator, for which the condition G>0:

$$
\begin{aligned}
&numerator\\
&= C_1 G\left\{\begin{array}{l}\left[2C_2\left(f_h(G)\big|_{\omega=Const}\right)^2 + 2C_3\, f_h(G)\big|_{\omega=Const} + C_3 G \frac{\partial f_h(G)}{\partial G}\Big|_{\omega=Const}\right] f_P(G)\big|_{\omega=Const} - \\ \left[C_2 G\left(f_h(G)\big|_{\omega=Const}\right)^2 + C_3 G\, f_h(G)\big|_{\omega=Const}\right]\frac{\partial f_P(G)}{\partial G}\Big|_{\omega=Const}\end{array}\right\}
\end{aligned}
\tag{43}
$$

Both the thermal function, *fh*(G), and the hydraulic function, *fP*(G), exhibit a power-law dependence on the mass flux G. These relationships can be expressed as:

$$
\begin{aligned}
f_h(G)\big|_{\omega=Const} &= D_1 G^a\\
\frac{\partial f_h(G)}{\partial G}\Big|_{\omega=Const} &= a D_1 G^{a-1}\\
f_P(G)\big|_{\omega=Const} &= D_2 G^b\\
\frac{\partial f_P(G)}{\partial G}\Big|_{\omega=Const} &= b D_2 G^{b-1}
\end{aligned}
\tag{44}
$$

where:

a, b: index of G, which is related to the other variables, but has a range of values:

$a \in[-0.13, 0.19]$

$b \in[-0.196, 0.376]$

$-2<a<b<1$

D_1, D_2: functions associated with other variables are considered as constants.

Substituting Eq. 44 into Eq. 43 gives:

$$
\begin{aligned}
&numerator =\\
&= C_1 G\left[\begin{array}{l}\left(2C_2 D_1^2 G^{2a} + 2C_3 D_1 G^a + aC_3 D_1 G^a\right) D_2 G^b - \\ \left(C_2 D_1^2 G^{2a} + C_3 D_1 G^{a+1}\right) b D_2 G^{b-1}\end{array}\right]\\
&= C_1 D_1 D_2 G^{a+b+1}\left\{\left[2C_2 D_1 G^a + (2+a) C_3\right] - \left(bC_2 D_1 G^{a-1} + bC_3\right)\right\}
\end{aligned}
\tag{45}
$$

Given the established conditions that b<2<(2+a) and $G^{a-1}<G^a$ for any G>1, the numerator is consequently always positive. This result implies that:

$$
numerator = C_1 D_1 D_2 G^{a+b+1}\left\{\left[2C_2 D_1 G^a + (2+a) C_3\right] - \left(bC_2 D_1 G^{a-1} + bC_3\right)\right\} > 0
\tag{46}
$$

Thus, the partial derivative $\frac{\partial\left(\frac{W}{Eu}\right)}{\partial G}$ is always greater than zero for any G>1. This result indicates that for all practical conditions where the mass flux exceeds unity, the performance index *W/Eu* increases monotonically with respect to G. Therefore, its theoretical maximum is achieved as G approaches infinity($G \to \infty$).

$$
\left(\frac{W}{Eu}\right)_{G,\max}\Bigg|_{\substack{W_r = Const\\ \omega = Const}} = \lim_{G\to\infty}\frac{C_1 D_1 G^{a+2}}{C_2 D_2 G^{a+b} + C_3 D_2 G^b} = \infty
\tag{47}
$$

That is, *W/Eu* diverges with respect to G. In summary, since the *W/Eu* index exhibits a monotonic dependence on both W_{r} and G, no internal optimal point exists within the defined parameter space. The theoretical maximum must therefore lie at the boundary condition defined by:

$$
\left(\frac{W}{Eu}\right)_{(W_r, G),\max}\Bigg|_{\omega} = A_0 \frac{\left(A_1 + A_3 r_{HW}\right) G_{\max}{}^{a-b+2}}{D_1(\omega) G_{\max}{}^a\left(A_4 + A_5 r_{HW} + A_6 r_{HW}{}^2\right) + A_7 + A_9 r_{HW}{}^2}\frac{D_1(\omega)}{D_2(\omega)}\Bigg|_{\omega}
\tag{48}
$$

That is, within the constraints of the operational domain, the *W/Eu* index attains its maximum value as $W_{\mathrm{r}} \to 0$ and G approaches its upper bound, $G_{\max}$.

CONCLUSION

In this study, a theoretical framework for evaluating the comprehensive thermo-hydraulic performance of condensation in horizontal rotating channels was established. A novel dimensionless index, *W/Eu*, was formulated as a function of key design parameters, namely channel spacing (W_{r}) and steam mass flux (G) through a rigorous first-order optimization process and the response of this index to variations in these parameters was determined, revealing the conditions for optimal performance.

The analysis demonstrated that the *W/Eu* index exhibits a clear monotonic dependence on both variables. Specifically, the index decreases monotonically as channel spacing (W_{r}) increases, indicating that its theoretical maximum is achieved as W_{r} approaches zero. Conversely, the index increases monotonically with steam mass flux (G), ultimately diverging as G approaches infinity.

These findings lead to a definitive conclusion for system optimization: within a given operational domain, the theoretical maximum for the comprehensive performance index, *W/Eu*, is located at the boundary condition of $W_{\mathrm{r}} \to 0$ and $G \to G_{\max}$. This implies that for the practical design of horizontal rotating heat exchangers, maximizing the overall flow and heat transfer performance is achieved by minimizing the inter-channel spacing and maximizing the steam mass flux, subject to the constraints of mechanical strength and operational feasibility. This work provides theoretical guidance for the design of a next-generation multi-channel cylinder dryer, while also paving the way for more efficient and sustainable paper production technologies.

ACKNOWLEDGEMENTS

The study is supported by Natural Science Research Start-up Fund of Xi'an Aeronautical Polytechnic Institute (2024XHQDJ02).

LITERATURE CITED

1. Choi, S.U.S., Yu, W., France, D.M., et al., *TAPPI J.* 84(2): 1(2001).
2. Shin, J.H., Hwang, K.S., Jang, S.P., et al., *Drying Technol.* 29(1): 47(2010). https://doi.org/10.1080/07373937.2010.482688.
3. Yang, P., Cao, X., Liu, J., et al., *Int. J. Heat Mass Transfer* 224: 125257(2024). https://doi.org/10.1016/j.ijheatmasstransfer.2024.125257.
4. Lee, B.-M., Gook, H.-H., Lee, S.-B., et al., *Int. J. Refrig.* 128: 71(2021). https://doi.org/10.1016/j.ijrefrig.2020.12.025.
5. Li, Q., Guangming, C., Qin, W., et al., *Int. J. Heat Mass Transfer* 187: 122524(2022). https://doi.org/10.1016/j.ijheatmasstransfer.2022.122524.
6. Yan, Y., Dong., J., Ren, T., et al., *Proc. Inst. Mech. Eng. Part A* 235(5): 1131(2021). https://doi.org/10.1177/0957650920972229.
7. Alnakeeb, M.A., El-Maghlany, W.M., Teamah, M.A., et al., *Exp. Heat Transfer* 33(3): 245(2019). https://doi.org/10.1080/08916152.2019.1625468.
8. Sohankar, A., Joulaei, A., and Mahmoodi, M., *Int. J. Therm. Sci.* 172: 107259(2022). https://doi.org/10.1016/j.ijthermalsci.2021.107259.
9. Gu, Y., Gong., L., Yali, G., et al., *Int. J. Refrig.* 144: 275(2022). https://doi.org/10.1016/j.ijrefrig.2022.08.001.
10. Deshmukh, R.G., Zanwar, D.R., Joshi, S.S., et al., *Mater. Today: Proc.* (2023). https://doi.org/10.1016/j.matpr.2023.08.220.
11. Wang, Z., Turan, A., and Craft, T., *Thermo* 3(1): 127(2023). https://doi.org/10.3390/thermo3010009.
12. Chiu, H.-C., Jang, J.-H., Yeh, H.-W., et al., *Int. J. Heat Mass Transfer* 54(1-3): 34(2011). https://doi.org/10.1016/j.ijheatmasstransfer.2010.09.066.
13. Pan, Y.-H., Zhao, R., Fan, X.-H., et al., *Int. J. Heat Mass Transfer* 163: 120461(2020). https://doi.org/10.1016/j.ijheatmasstransfer.2020.120461.
14. Vaisi, A., Javaherdeh, K., and Moosavi, R., *Int. J. Heat Mass Transfer* 182: 121968(2022). https://doi.org/10.1016/j.ijheatmasstransfer.2021.121968.
15. Li, H.T., Wang, N., He., S., et al., *Appl. Therm. Eng.* 216: 119112(2022). https://doi.org/10.1016/j.applthermaleng.2022.119112.
16. Zhang, J., Ren, Y., Lihong, Z., et al., "Analysis of influencing factors of heat transfer performance of heat pipe heat exchanger," *Int. Conf. Energy Environ. Technol.*, IEEE, New York, 2009.
17. Sun, D.C., Yuan, D.W., Qiu, Z.C., et al., *Ann. Nucl. Energy*, 204: 110571(2024). https://doi.org/10.1016/j.anucene.2024.110571.

ABOUT THIS PAPER

Cite this article as:
Wang, S., Guo, H., and Wang, J., *TAPPI J.* 25(5): 310(2026). https://doi.org/10.32964/TJ25.5.310

DOI: https://doi.org/10.32964/TJ25.5.310

ISSN: 0734-1415

Publisher: TAPPI Press

About this journal

ABOUT THE AUTHORS

To investigate the heat transfer performance of a multi-channel cylinder dryer, we established a functional relationship for the novel dimensionless index, *W/Eu*, presented here with respect to channel spacing and steam mass flux. This was followed by a theoretical optimization analysis.

The most difficult part of the study was the theoretical analysis of the dimensionless index *W/Eu* for comprehensive evaluation of the thermo-hydraulic performance. It was discovered that the comprehensive performance indicator *W/Eu* exhibits a monotonically dependent relationship with respect to channel spacing and steam mass flux. Its theoretical maximum value consistently resides under the boundary conditions of minimum spacing and maximum mass flux.

For mills, a next-generation MCD could enhance the efficiency of the paper manufacturing process. Our next step is to study how flow patterns impact heat transfer performance.

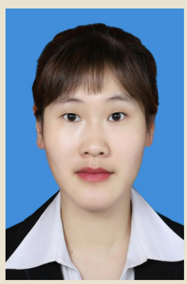

S. Wang

H. Guo

J. Wang

S. Wang is a lecturer in the College of Automation Engineering at Xi'an Aeronautical Polytechnic Institute in Xi'an, China. H. Guo is a researcher and J. Wang is associate professor in the College of Mechanical and Electrical Engineering at Shaanxi University of Science and Technology in Xi'an, China. Email Wang at jywang@sust.edu.cn.

18. Ammar, S.M., Abbas, N., Abbas, S., et al., *Int. J. Heat Mass Transfer* 134: 366(2019). https://doi.org/10.1016/j.ijheatmasstransfer.2019.01.047.
19. Sakamatapan, K., Kaew-On, J., Dalkilic, A.S., et al., *Int. J. Heat Mass Transfer* 64: 976(2013). https://doi.org/10.1016/j.ijheatmasstransfer.2013.04.020.
20. Wang, S., Dong, J., Guo, H., et al., *Appl. Therm. Eng.* 213: 118769(2022). https://doi.org/10.1016/j.applthermaleng.2022.118769.
21. Wang, S., Dong, J., Guo, H., et al., *Therm. Sci.* 26(6B): 5253(2022). https://doi.org/10.2298/TSCI220313111W
22. Cavallini, A., Del Col, D., Doretti, L., et al., *Heat Transfer Eng.* 27(8): 31(2006). https://doi.org/10.1080/01457630600793970
23. Kim, S.-M. and Mudwar, I., *Int. J. Heat Mass Transfer* 55(11-12): 3246(2012). https://doi.org/10.1016/j.ijheatmasstransfer.2012.02.047.
24. Wang, S., Guo, H., Wang, J., et al., *Therm. Sci. Eng. Prog.* 57: 103114(2025). https://doi.org/10.1016/j.tsep.2024.103114.